THE UNIVERSITY OF CHICAGO

DEPOSITION AT PINNED AND DEPINNED CONTACT LINES: PATTERN FORMATION AND APPLICATIONS

A DISSERTATION SUBMITTED TO

THE FACULTY OF THE DIVISION OF THE PHYSICAL SCIENCES

IN CANDIDACY FOR THE DEGREE OF

DOCTOR OF PHILOSOPHY

DEPARTMENT OF PHYSICS

BY

ROBERT D. DEEGAN

CHICAGO, ILLINOIS

DECEMBER 1998

For Ola, Thomas, and Martin

ACKNOWLEDGMENTS

Sid Nagel has been a friend, a counselor, and a mentor. He has shared with me and inspired me with his vision of science. I am deeply grateful.

My family has been a bottomless well-spring of love and support. I could not have done this without them.

I also want to thank Tom Witten and Todd Dupont for many fruitful and thought-provoking discussions, Jennie Traschen and Po-zen Wong for getting me to the University of Chicago in the first place, the members of the James Franck Institute–Sue Coppersmith, David Grier, Philippe Guyot-Sionnest, Heinrich Jaeger, Leo Kadanoff, and Gene Mazenko–who have helped by listening, nudging me in the right direction, providing encouragement, and sharing their expertise, and my friends and colleagues–Olgica Bakajin, Shaun Blanton, Jan Chabala, Itai Cohen, John Crocker, Georges Debregeas, Sergie Esipov, Jim Knight, Margret Hines, Anka Hussmann, Bob Leheny, Ward Lopez, Andy Marcus, Melica Medved, Narayanan Menon, Dan Mueth, John Wahl, and Rob Wickham–who helped in countless ways to get to this point and to enjoy the ride.

The staff of the JFI–Jeanetta Allen, Rosemary Garrison, Mark Menedez, Mike Pearson, John Phillips, Stás Potocki, Joyce Rucker, and Melva Smith–is wonderful. I want to thank them for the parties, easing the bureaucratic process, indis-

pensable assistance with building experiments, and generally fostering a great working environment.

Last, I want to thank Nobuko McNeil for all her care through my graduate career.

TABLE OF CONTENTS

LIST OF FIGURES

ABSTRACT

Ring formation in an evaporating sessile drop is a hydrodynamic process in which solids dispersed in the drop are advected to the contact line. After all the liquid evaporates, a ring-shaped deposit is left on the substrate that contains almost all the solute. Here I show that the drop can itself provide one of the essential conditions for ring formation to occur: contact line pinning. The strength of this self-pinning is a power law in the initial concentration of the solution. Furthermore, I show that when self-induced pinning is the only source of pinning an array of patterns–that include cellular and lamellar structures, sawtooth patterns and Sierpinski gaskets–arises from the competition between dewetting and contact line pinning. I also demonstrate that structures 100 nm in size can be fabricated using ring formation.

CHAPTER 1

INTRODUCTION

A fluid droplet on a solid surface is ostensibly so simple a physical system that one might suppose that all its behavior is thoroughly understood. Despite countless studies going back at least 200 years 1, issues about the phenomena occurring at the contact line, defined as the line beyond which the solid is wet, continues to engage the interest of the scientific and engineering community. One such issue is contact line pinning 2, 3. Looking through a window after a rainstorm one is struck by the fact that droplets though on a vertical surface nonetheless defy gravity. The force that holds them in place arises from pinning of the contact line by irregularities, such as roughness or chemical heterogeneity, on the surface of the glass 4. Here I explore how the contact line can become pinned due to solute within the liquid that corrupts the substrate. The capacity of solute to alter the surface properties of the substrate is not a new phenomenon but in ring-forming drops it achieves a new scale in strength because the solute accumulates at the contact line which is precisely where it has the greatest effect.

This work is an extension of an earlier study in which my colleagues and I developed and tested experimentally a theory for the formation of rings in a drying drop [5, 6]. A common manifestation of this phenomenon is the brown ring left

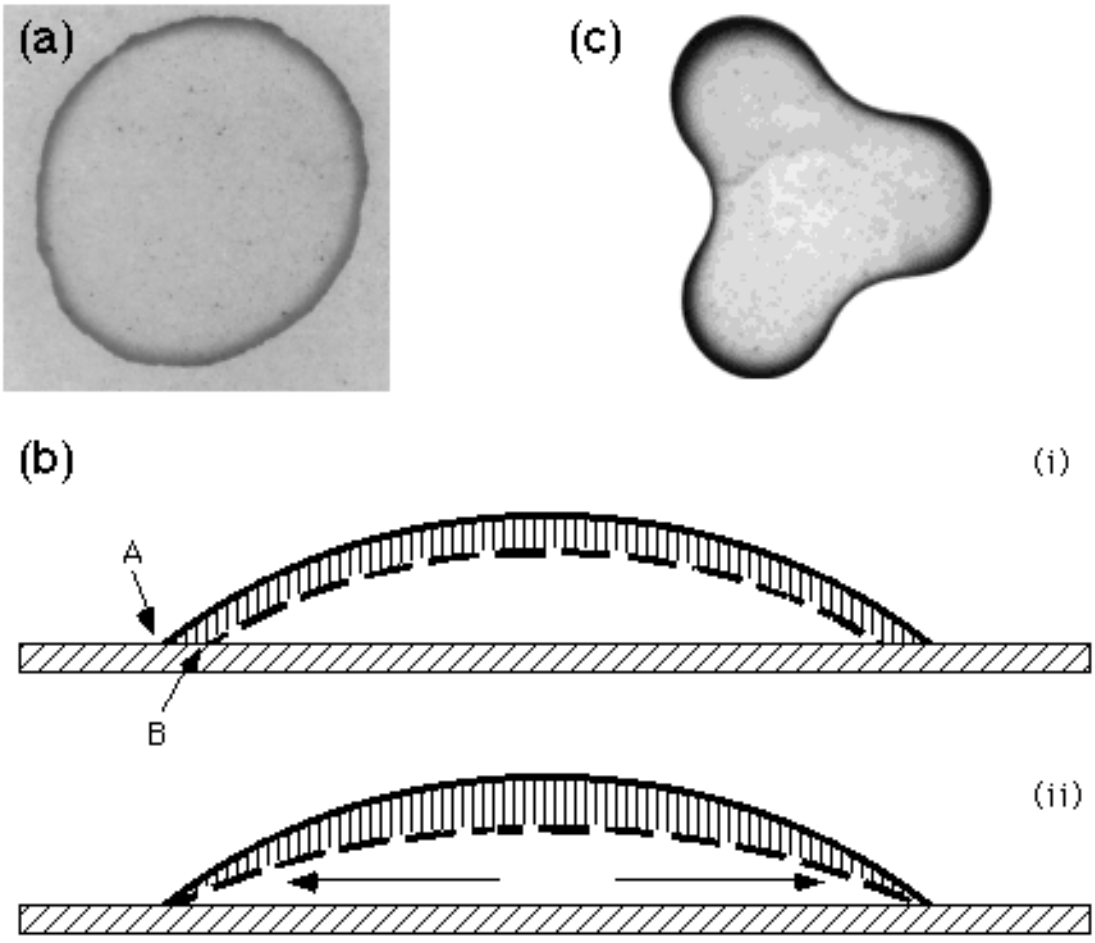

Figure 1 Coffee ring phenomenon. (a) A photograph of a dried coffee drop. The dark perimeter is produced by a dense accumulation of coffee particles. (b) Schematic illustration of the origin of the advective current. (i) If the contact line were not pinned, uniform evaporation would remove the hashed layer, the interface would move from the solid line to the dashed line, and the contact line would move from A to B. However, if the contact line is pinned then the retreat from A to B is not possible and there must be a flow that replenishes the lost fluid. (ii) Shows the actual motion of the interface and the compensating current. (c) This misshapen coffee deposit is indicative of the limited control that is possible with ring formation.

when a drop of coffee dries on a counter top (see Fig. 1(a)). We found that contact line pinning and evaporation are sufficient conditions for ring formation. Since these are common and generic conditions, ring formation often occurs whenever a liquid with solid constituents evaporates. The ring forms because the contact line cannot move. Therefore, when evaporation removes liquid from around the contact line a flow develops to keep the substrate wet up to that point (see Fig. 1(b)). The solute in the drop is dragged to the contact line by this flow, where it accumulates into as a ring-like formation.

The substrate by itself cannot keep the contact line pinned indefinitely. In [5, 6] it was speculated that the accumulation of solid components at the contact line perpetuates the pinning of the contact line. Here I will refer to this process as "self-pinning" because of the bootstrapping that is intrinsic to ring formation: some preexisting conditions on the substrate temporarily anchors the contact line, this permits the start of ring formation, and the additional growth increases the energy barrier the contact line must surmount to move. In this thesis I will show that self-pinning does occur and that it gives rise to pattern formation. I will also elucidate how ring formation can be used for microfabrication of small structures.

CHAPTER 2

SELF PINNING

In order to test the hypothesis of self-pinning, I isolated the effects of solute pinning by using a smooth homogenous substrate. Freshly cleaved mica provides such a surface. The substrates were prepared from a slab of mica by prying open a corner and introducing a drop of deionized water. The water cleaves the interlayer potassium bond and if done properly produces an atomically flat surface. A minimal amount of water was used to avoid excessive contamination of the surface. The sheets were left in open air until they dried which typically took less than 20 seconds, briefly exposed to the flame of a Bunsen burner, and placed on a copper plate to cool. The sheets were used as soon as their temperature returned to normal.

The mica substrates I used were not necessarily atomically flat. The smoothness with which a liquid sweeps across the surface provides a test of this. I observed the behavior of filtered deionized water deposited on the mica. (As with all fully wetting liquids, in addition to the macroscopic contact line there is also a microscopic line due to the precursor film that extends beyond the macroscopic contact line. The contact line referred to herein will always be the macroscopic contact line.) The radius of such a drop, with an initial volume 0.5 μl, versus time is plotted in Fig 2. Initially the drop spread and after it reached a maximum radius of 2 mm it shrunk

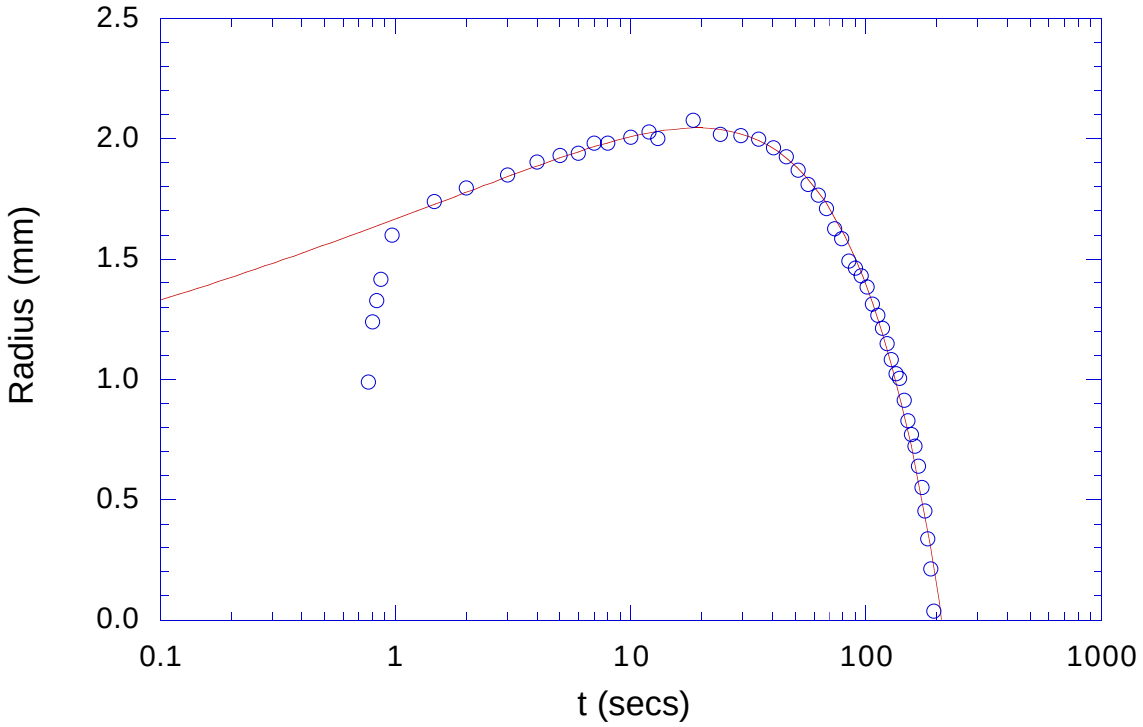

Figure 2 Water drop on mica. Plot of the radius of a water drop (mm) drying on a mica substrate versus time. The line running through the data is best fit to the form $R(t) = R_o\ t^{1/10}(1 - t/t_f)$. The first five data points were ignored during the fitting procedure.

continuously to zero size. The smoothness of the data in Fig. 2 is a measure of the smoothness of the substrate. Repeated trials indicated that the substrates had only 1 pinning site per cm^2.

The drops in the experiments that follow were made from a 2% solid volume fraction colloidal suspension of sulfate-terminated polystyrene microspheres dyed yellow-green fluorescent acquired from Interfacial Dynamics, Portland, Oregon. The colloid was synthesized by a surfactant-free method which minimizes the presence of amphiphilic molecules. I used two different microsphere diameters: 1 μm and 0.1 μm.

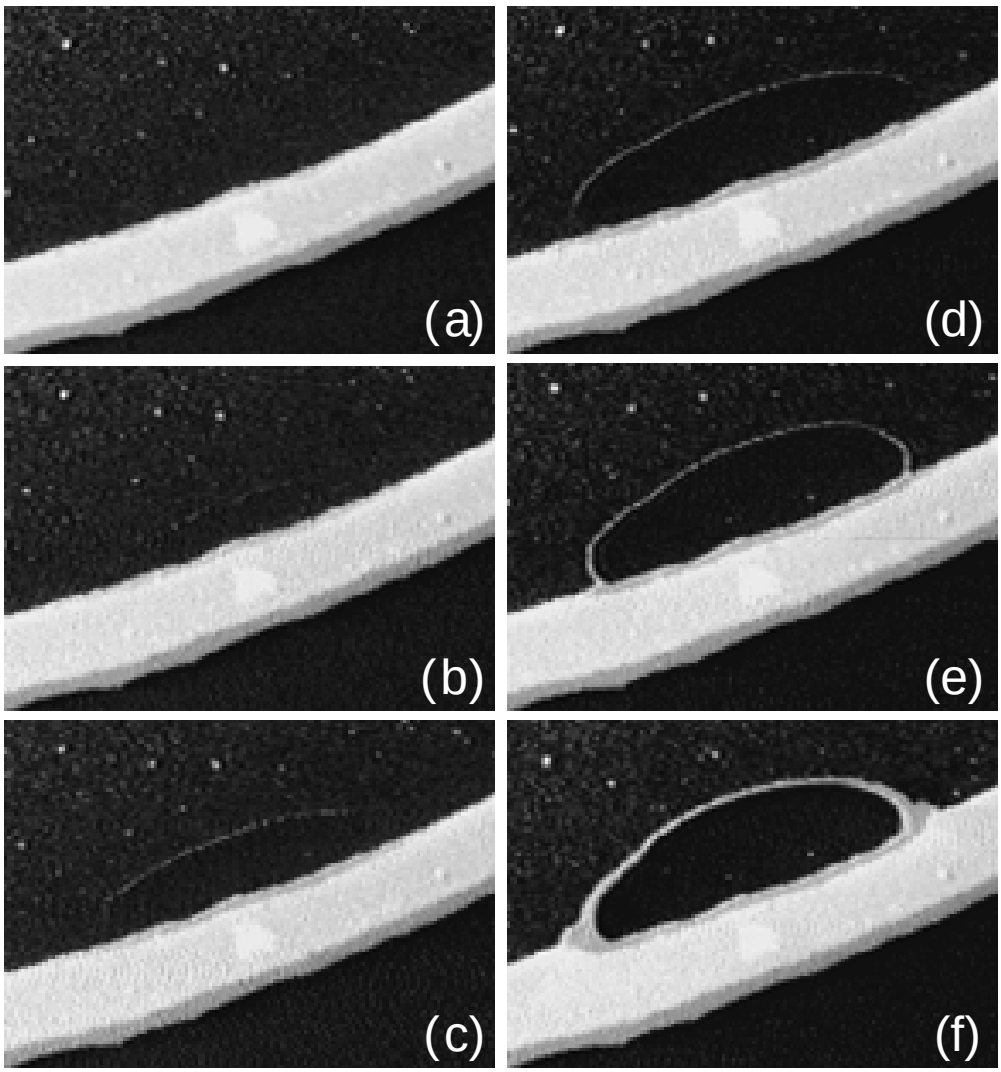

Figure 3 Depinning Event. Photographic sequence demonstrating the formation of a hole. The view is from above and the solid white band in the lower part of the frame is the ring; the rest of the drop is above the ring. The hole is created, expands and eventually contained by the accumulation of microspheres along its edge. The portion of the ring next to the hole remains wet throughout the period covered by the figure. The flow inside the drop remains outward directed even when the contact line is retreating. (The backward motion of some of the larger particles appears to contradict this statement. However, these particles are clamped between the liquid surface and the substrate so that their motion is governed by the the interface's motion, and hence by the contact line's motion, instead of by the fluid flow.) The times for frames (a) through (f) are t = 0, 0.23, 0.50, 0.83, 1.87, 5.90 seconds, respectively. The major axis of the hole is approximately 150 μm.

Volume fractions different from 2% were made by diluting the colloid with deionized water or by sedimenting the microspheres in a centrifuge and decanting the clear liquid.

When placed on mica, a drop of colloid will grow quickly to its largest size, much like the drop of pure water shown in Fig. 2. For example, a 0.5 μl drop will spread to a maximum radius of 2 mm leaving the center height at approximately 150 μm. Unlike a drop of pure water, the drop of colloid does not shrink after reaching its maximum size. Instead it remains at its maximum size for a substantial fraction of the drying time. Nadkarni and Garoff [7] showed that a single microsphere attached to the surface can pin the contact line. The same process appears to occur here but at a larger scale. The microspheres jam into the wedge of fluid next to the contact line, preventing it from retracting. A ring is formed during this initial pinned stage. At late times, the liquid pulls away from the ring and shrinks down to zero radius. During this phase, segments of the contact line continually switch between a pinned and a depinned state, leaving a trail of deposits which can be highly regular. The depinning process begins with the nucleation of a dry spot along the inner edge of the ring (see Fig. 3). Gradually more dry spots develop until the contact between the liquid and the ring is completely severed. I measured the fraction of time during which the drop remained pinned and the width of the thinnest portion of the ring.

To measure the time of the initial pinned state, the drop was dried on an analytical balance and the mass as a function of time was recorded. A magnified image

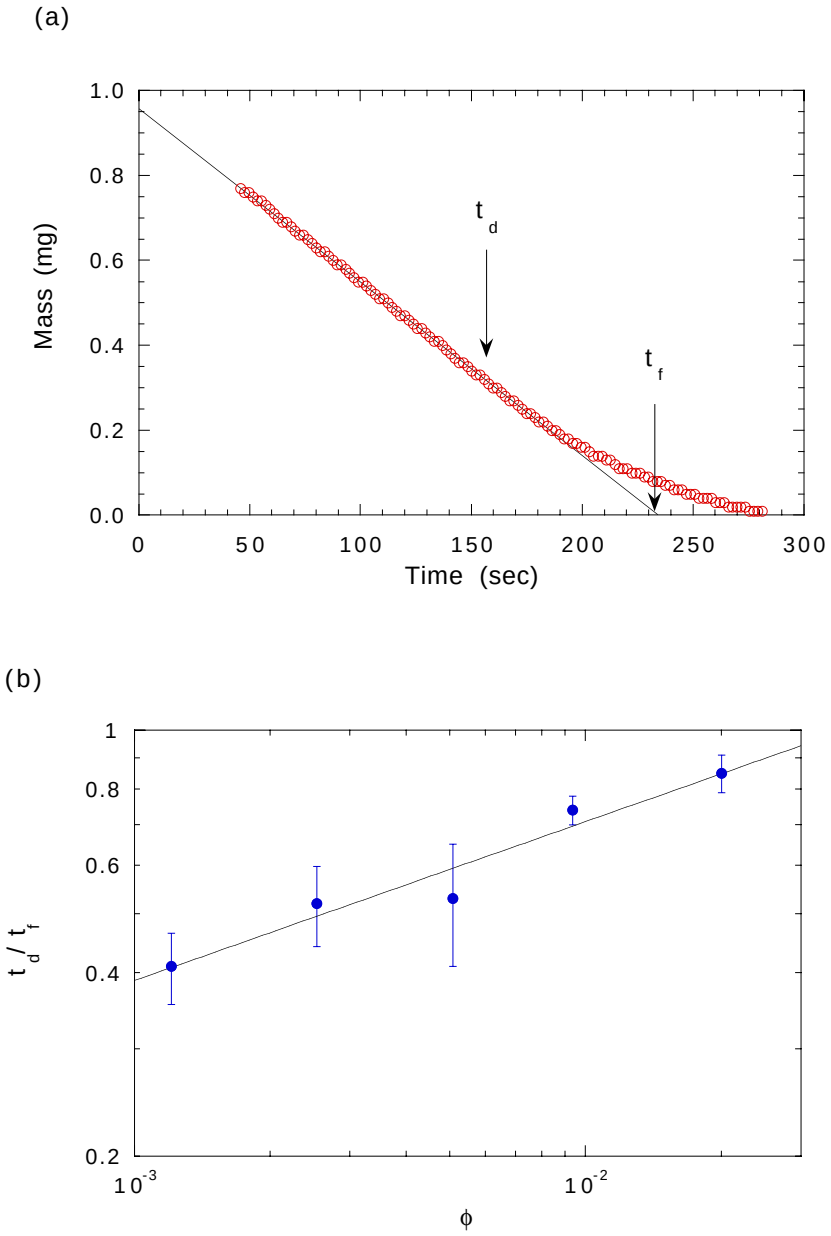

Figure 4 Plot of depinning time versus concentration. (a) Mass of a drying drop versus time. The early time data is suppressed because it contains transients due to the settling time of the balance. The arrows indicate the depinning time, labeled t_d, and the extrapolated drying time, labeled t_f. The depinning time is determined by the first appearance of a hole, as in Fig. 3, near the contact line. (b) Depinning time normalized by the extrapolated drying time versus concentration. The line running through the data is a best fit to a power law which yields an exponent of 0.26 ± 0.08.

of the drop was acquired using a CCD camera and was used to visually monitor the state of the drop. The depinning time, t_d, was measured when the first hole forms. The effective total drying time of the drop, t_f, was determined by a linear extrapolation of the mass versus time plot to zero as shown in Fig 4(a). Since the evaporation rate depends only on the radius of the drop, t_f is equal to the total drying time that would be obtained if the drop remained pinned throughout its lifetime. The depinning time, normalized by t_f, versus the initial solid volume fraction, ϕ, is plotted in Fig. 4(b). The data is approximately linear on a log-log scale and a best-fit to a power law yields an exponent of 0.26 ± 0.08. For concentrations below 0.1% there was insufficient contrast in the video image of the drop to determine the depinning time.

The self-pinning process was also characterized by measuring as a function of initial concentration the width of the ring at its narrowest point. When a depinning event occurs the ring at that point ceases to grow and so the thinnest portion of the ring indicates where the first depinning event occurred. The volume of each drop varied because of inaccuracies intrinsic to pipetting small volumes. Therefore, the width of the ring, w_d, was normalized by the drop radius, R, to compensate for different size drops. Fig. 5(a) shows a plot of w_d/R versus ϕ. For drops of equal volume the average radius maximum showed a slight concentration dependence, increasing by about 10% when the concentration changed by a factor of ten. The different data sets plotted correspond to 0.1 and 1 μm particle sizes. The two data sets coincide and, therefore, for clarity they are offset from each other by multiplying the 0.1 μm data

by a factor of five. I was unable to obtain data for particle sizes outside of this range because larger particles sediment too quickly and smaller particles are commercially unavailable in a surfactant-free suspension. Both data sets are well fit by a power law which for the 0.1μm beads gives an exponent of 0.78 ± 0.10 and for the 1μm beads gives an exponent of 0.86 ± 0.10. Within the experimental uncertainty these two exponents are equal.

If changing the size of the drop only changes its scale and not its shape then the width of the ring should scale with the radius. That is, the volume of the wedge-shaped ring will be proportional to Rw^2 and this volume must contain an amount of solute proportional to volume of the drop R^3 so that $w \propto R$. To explicitly test this assumption, I measured w_d and R for drops of different sizes but the same concentration. The results plotted in Fig. 5(b) demonstrate that the w_d scales with R over this range of radii.

It is not readily apparent that the width data of Fig. 5 are consistent with the depinning time data of Fig. 4. A rough estimate of the width as a function of time can be gotten by assuming that the ring is an annulus with a cross-section shaped like a right triangle (i.e. a wedge). Therefore, its volume is:

$$V_r = \pi R w^2 \theta_c \tag{2.1}$$

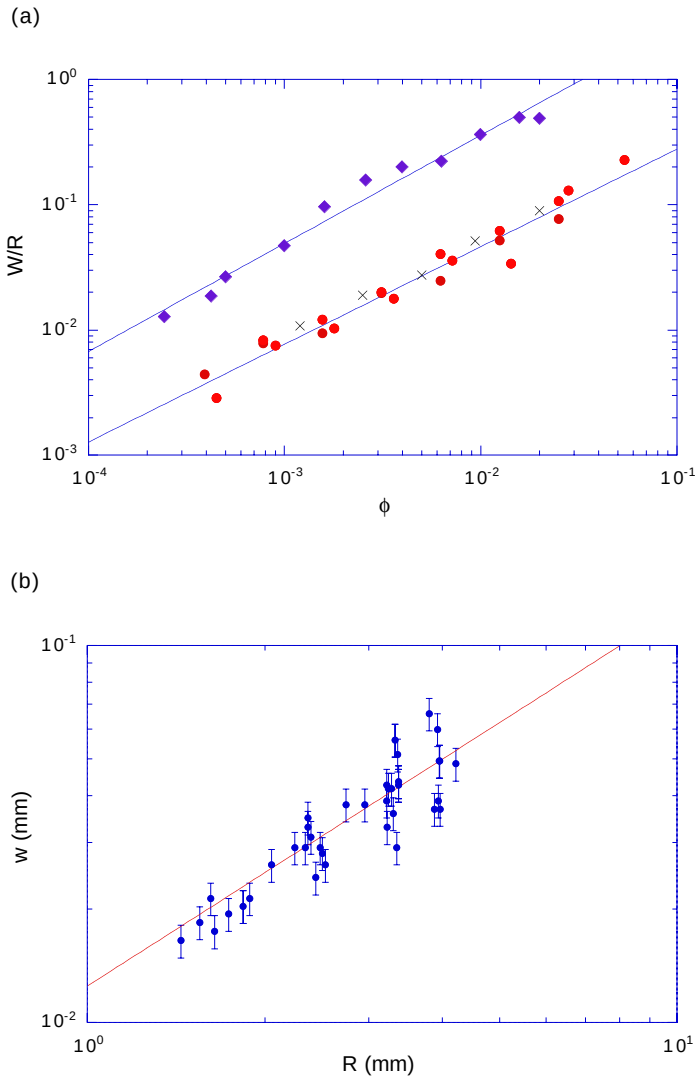

Figure 5 Width of ring at depinning versus concentration. (a) The width of the ring at depinning normalized by the drop radius versus the concentration. The upper data set is for 0.1μm microspheres and the lower one is for 1μm microspheres. The 0.1μm data set has been multiplied by 5 to separate the two data sets. A best fit to a power law gives an exponent of 0.78 ± 0.10 for 0.1μm microspheres and 0.86 ± 0.10 for the 1 μm microspheres. The crosses ($\times$) correspond to the width calculated using the model given in the appendix and using the data from Fig. 4(b). (b) The width at depinning for drops of different sizes but of equal initial concentration (1.56×10^{-3} volume fraction) plotted against the radius. The line running through the data is a fit to the functional form $w = aR$.

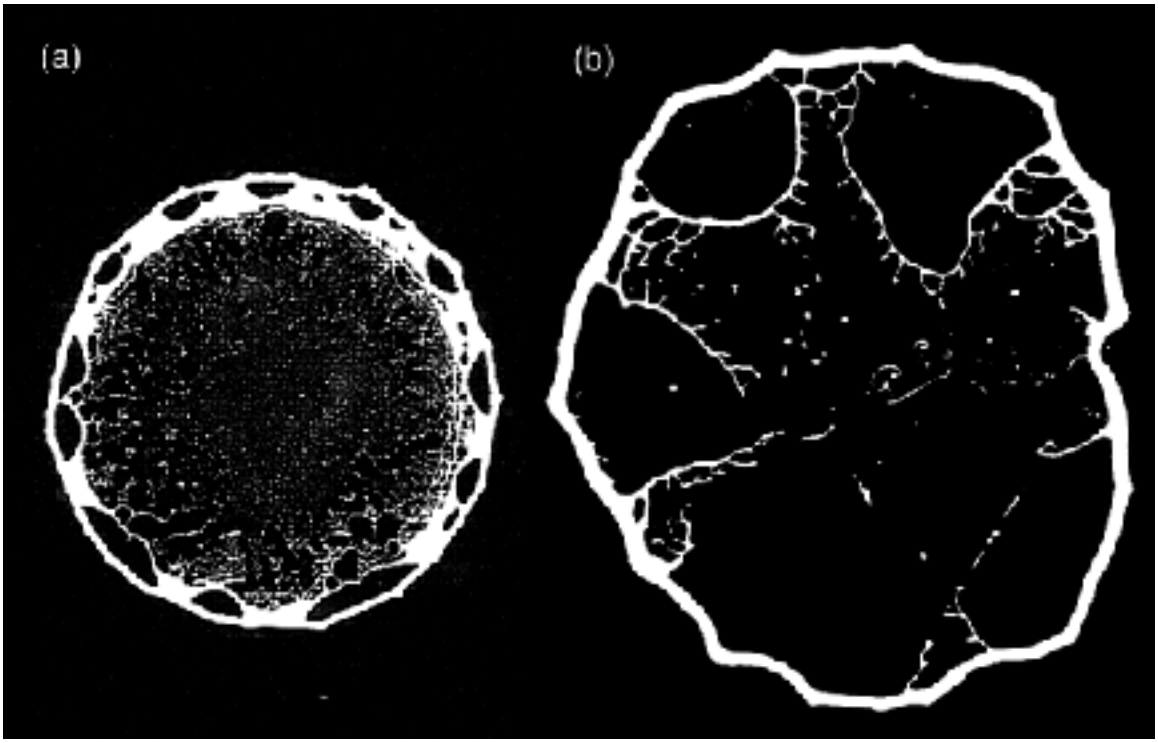

Figure 6 Comparison of fast versus slow drying. (a) The deposit left by a drop dried in the open air. (b) The deposit left by a drop, made from the same solution as (a), dried in the chamber described in text. The drying time is 20 times longer for (b) than for (a). The images have the same scale and so the photographs indicate that (b) is approximately twice as wide as (a). This is the result of the drop in (b) spreading for a longer time period than (a) before evaporation truncated the spreading process. Also, the images indicate that the size of the arches in (b) are much larger than those in (a).

with the approximation that $\tan\theta_c \simeq \theta_c$ which applies to the thin drops in my experiments. In prior work 6, the volume of the ring, V_r, as a function of time was shown to be:

$$V_r = p^{-1}\frac{\pi R^3 \theta_c}{4}\phi\left[1-(1-t/t_f)^{3/4}\right]^{4/3} \tag{2.2}$$

where the prefactor is the total amount of solute in the drop at $t = 0$ multiplied by the inverse of the packing fraction, p. The formula indicates that initially there is

no ring ($V_r(t = 0) = 0$), and that the final ring contains all the solute. Combining Eq. 2.1 and 2.2 produces:

$$w/R = \sqrt{\frac{\phi}{4p}}\left[1 - (1 - t/t_f)^{3/4}\right]^{2/3} \sim \sqrt{\phi}\, t^{2/3} \tag{2.3}$$

for $t \ll t_f$. At the first depinning event $w_d = w(t_d) \sim \sqrt{\phi}\, t_d^{2/3}$. Using the experimental result $t_d \sim \phi^{0.26\pm0.08}$ yields $w_d \sim \phi^{0.67\pm0.05}$. This result is consistent within experimental uncertainty with the width data of 0.1 μm microspheres but not with the width data of 1 μm microspheres.

Equation 2.3 underestimates the growth rate of the ring because the ring's actual shape is different from that of a wedge. Consider the innermost edge of the ring to be the interface between a solid (packed microspheres) and a liquid. The speed with which the interface moves inward is determined by how fast microspheres arrive and how highly they can be stacked. The height of the stacking depends on the angle of the liquid surface relative to the substrate; a larger angle can accommodate a higher stacking of microspheres. Since this angle must be smaller than the initial contact angle and is, furthermore, decreasing in time, the ring will be wider than that calculated above. A more precise calculation for the ring width which explicitly includes the opening angle is given in the appendix. For each of the data points (ϕ, t_d) in Fig. 4(b), the differential equations in the appendix were numerically integrated from $t = 0$ through $t = t_d$, using ϕ as an input parameter. The crosses in Fig. 5(a)

correspond to the results of this integration. The agreement between the depinning time and width data is good.

These experimental results demonstrate that self-pinning does occur and that it has a predictable dependence on the initial concentration. It is worth emphasizing that contact line pinning due to the accumulation of microspheres is expected and has already been amply demonstrated by Nadkarni 7. What is novel about the pinning process in this system is that it arises from a self-organized of the pinning sites.

The formation of a hole is the first stage of depinning. A subset of possible mechanisms for its formation are dynamical instabilities. In order to determine the relevance of kinetic effects, I reduced the rate of evaporation so that dynamical quantities such as flow velocity and temperature gradients were reduced. To accomplish this, a drop was placed on a mica substrate and covered with a microscope slide in which a bowl about 2 cm wide and 2 mm deep was carved out. The drop was thus surrounded by a glass container which vented to the atmosphere solely through the gaps between the glass slide and the substrate. The drop took twenty times longer to dry than an identical drop drying in the open air. I found that the first hole appeared in the slow drying drop at the same effective time, t/t_f, as its rapidly drying counterpart. I concluded therefore that hole formation is not a dynamical effect.

The apparent lack of a dynamic signature at the onset of hole formation leaves open the possibility of a static criterion. The spontaneity with which holes

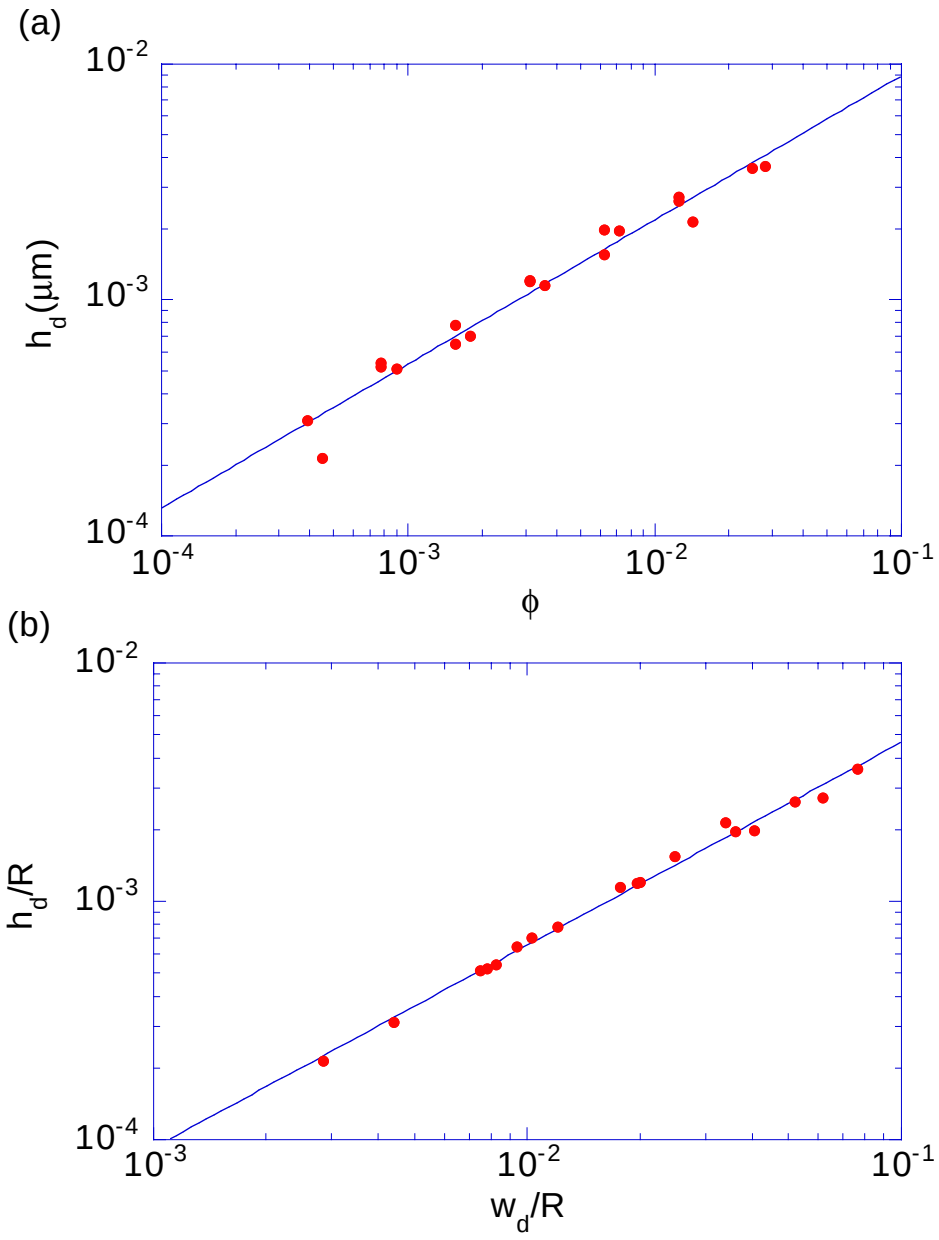

Figure 7 The height and angle of the ring at depinning. (a) the height of the ring at depinning in units of μm calculated using the results of the appendix and the data in Fig. 5. (b) The height at depinning versus w_d. The data is best fit by a power law with exponent of 0.85 ± 0.05.

form is reminiscent of nucleation and growth phenomenon. This suggests a static criterion might be based on energetic considerations. However, the ingredients in the energy balance are unclear considering that the depinning in a ring-forming drop is unusual in several respects. First, though the free energy of a water drop will decrease as it spreads over mica, the retraction shown in Fig. 2 is what one would expect if spreading were energetically unfavorable. In other words, though water wets mica it behaves as if though it were only partially wetting. Second, the depinning of a contact line from a surface asperity only involves a distortion of the contact line whereas the depinning in a ring-forming drops involves the creation of a new contact line. Third, though the hole clearly has a macroscopic contact line, the region within the hole is coated with a thin layer of liquid, i.e. the precursor film. Any explanation of the depinning must account for these effects.

To investigate the possibility of a static criterion I used the model in the appendix to calculate the height of the ring, h, and the angle of the free surface with respect to the substrate, Θ. In Fig. 7(a) the h versus ϕ is plotted. These data show that h is a strong function of ϕ. In Fig. 7(b) the h versus w is plotted. The data is best fit by a power law with an exponent of 0.85 ± 0.05. Since $dh/dw \approx \Theta$ this indicates that $\Theta \sim w^{-0.15\pm0.05}$ which together with the dependence of w on ϕ gives $\Theta \sim \phi^{0.12\pm0.05}$. Since this is a weak function of ϕ, it appears that Θ may be a good predictor of when the drop depins.

CHAPTER 3

THIN RINGS

Ring formation is a process by which particles suspended in a liquid self-assemble along the contact line of a drying drop. As shown in Fig. 1, the contact line, and therefore the shape of the ring deposit, can be manipulated to give a wide range of shapes. If deposits of submicron width can be formed, then this process may provide an alternative to conventional lithographic microfabrication. In principle, all one need do is pipette a dilute suspension of particles onto a substrate.

Pinning is essential for ring formation and given that a thin rings will provide almost no hinderance to contact line motion, it is necessary that the substrate be the primary source of pinning. To understand the evolution of the pinning that occurs in a drop, consider the contact angle on a plate when it is slowly immersed and retracted from a liquid. During immersion the contact line advances across the plate and the contact angle maintains a value θ_a called the advancing contact angle. Upon withdrawal of the plate, the contact line is temporarily pinned and the contact angle changes continuously from θ_a to a lower value θ_r called the retreating contact angle. Only after reaching this lower value does the contact line again begin to move. Similarly, a drop initially spreads until the contact angle decreases to θ_a. Thereafter the contact line remains pinned until evaporation removes sufficient liquid so that the

contact angle decreases to θ_r [8]. Therefore, the contact angle is the quantity that determines the dynamic behavior of the contact line.

Contact-line depinning is an obstacle to making very thin rings because the retreat of the contact line blurs or worse destroys the ring. To avoid this, I constructed the apparatus, depicted schematically in Fig. 8, that keeps the volume of the drop and therefore its contact angle constant. The apparatus works as follows: a drop of solution dries on a silicon substrate lying in the pan of an analytic balance (resolution: 20 μg). The mass of the drop is read into a computer where a proportional-integral-derivative algorithm is used to calculate the rate at which water should be added to the drop. On command from the computer pure water is injected into the drop in increments of 10 μg through a plastic pipette tip which is in contact with the liquid at the center of the drop. The flow inside the drop may be thought of as a conveyor belt. Liquid is removed by evaporation from the contact line region, the liquid deeper in the drop moves outward to take its place, and the "space" vacated at the center of the drop is filled with pure water. Like clarifying murky water by continuously adding clear water, eventually the drop contains little or no solute.

This procedure not only eliminates depinning but it also minimizes the speed at which the solid/liquid (i.e. ring/solution) interface advances towards the center of the drop. Since the contact angle is fixed the ring grows like a wedge. As shown in the previous chapter, a wedge-like ring grows inward at a slower rate than a ring whose shape is determined by the angle at which the liquid interface meets the solid

ring. Barring additional constraints, the contact angle should be kept at the highest possible value to minimize the rate at which the interface propagates.

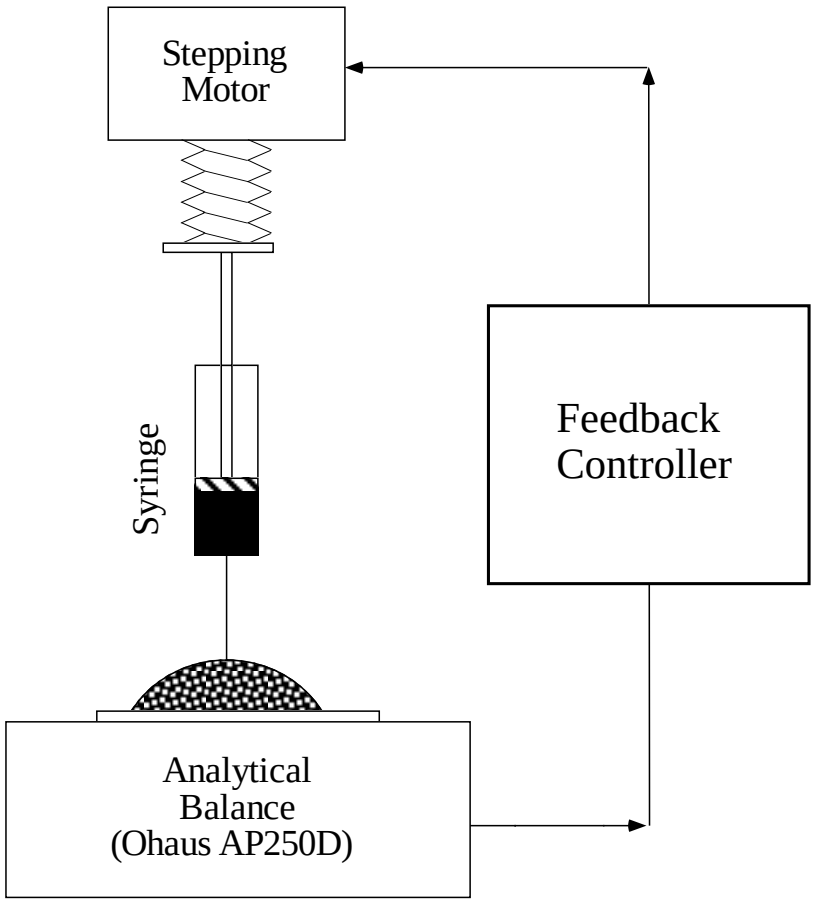

Figure 8 Schematic of the constant volume experiment. A drop sits on an analytic balance. The drop is kept at a constant volume by using the weight as the input for a feedback loop that regulates the amount of liquid injected into the drop.

The drops in these experiments were made from colloidal gold, with particle diameters of 40 nm and 15 nm, purchased from Polysciences, Warrington, Pennsylvania. The first step in the fabrication process is to pipette a 20 μl drop onto a flat silicon substrate lying in the pan of the balance. The drop spreads to a diameter of

approximately 6 mm. Five microliters are then withdrawn from the drop to lower the contact angle to a value between θ_a to θ_r. Lowering the contact angle provides a buffer so that fluctuations in the drops volume, which inevitable occur because of noise in the feedback loop, do not cause further spreading. The drop is left to dry and water is continually added to keep the volume fixed for eight hours. The feedback loop keeps the volume constant to within $\pm 1\%$. During the drying time 320 μl of pure water are added to the drop. After this time the drop is allowed to dry naturally.

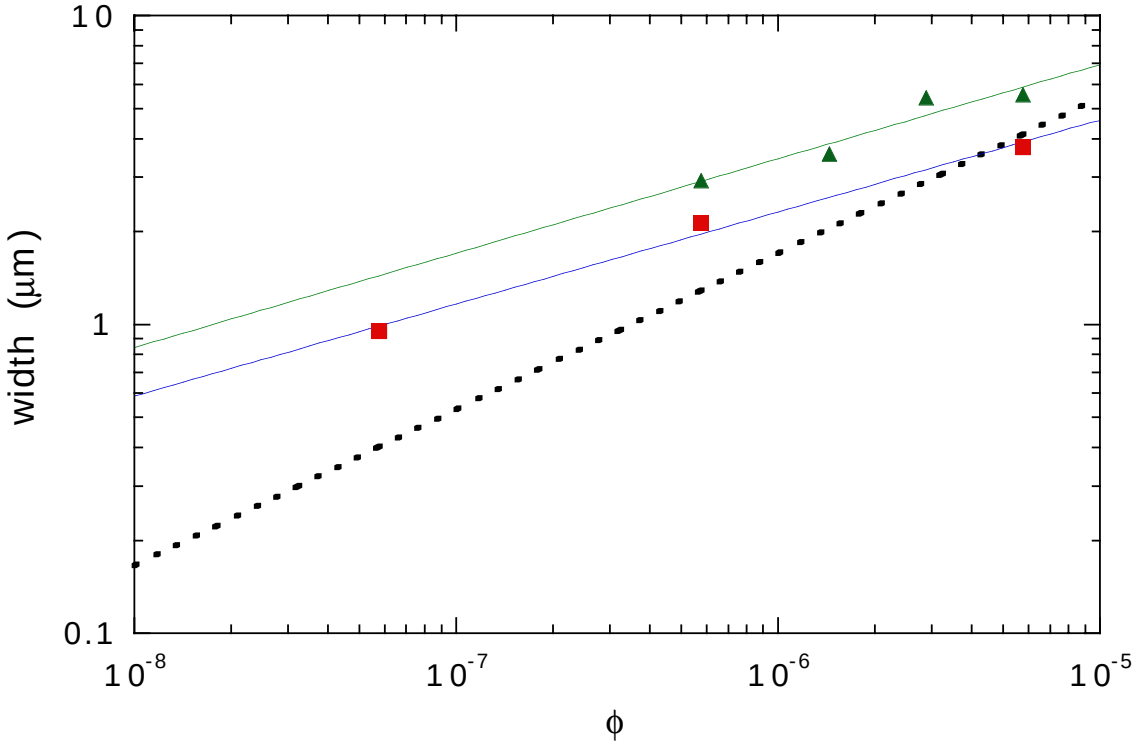

Figure 9 Width of gold ring. The width of the ring produced by the constant volume experiment plotted against the initial volume fraction of gold. The triangles correspond to rings formed from 40 nm particles and the squares correspond to rings formed from 15 nm particles. The lines running through the data are fits to a power law which in both cases gives an exponent of approximately 0.25. The dashed line is the width of the ring expected from the initial volume fraction of the solution

The width of the ring left on the substrate was measured using a scanning electron microscope (SEM). By decreasing the concentration of the initial drop, I was able to manufacture arbitrarily long structures with a minimum width of 500 nm. In the more dilute samples short ($\sim 1\mu$m) structures with a minimum width of 100 nm often can be found. Though these structures are reproducible their positioning along the contact line is uncontrolled. The width of fully reproducible and controllable rings, w_a, versus the initial volume fraction of gold is plotted in Fig. 9. The expected width, w_e, was calculated from the experimental parameters, assuming that all the solute was transfered to the ring as follows:

$$w_e = \sqrt{\frac{\phi V(0)}{p\pi R \tan\theta_c}} \tag{3.1}$$

where $V(0)$ is the initial volume of the drop, R is the radius of the drop, and p is the packing fraction. I used values of $V(0)$ =15 μl, R =3.0 mm, $\theta_c = 49^o$, and p =0.656 (the random close packed value). The expected width is plotted as a dashed line in Fig. 9. The actual ring width decays with decreasing concentration much more slowly than the expected width. The data is best fit with a power law which shows that rings of both 40 nm and 15 nm particles vary approximately as $w_a \sim \phi^\lambda$ with $\lambda \simeq 0.3$. In addition, below a certain concentration ($\phi < 5 \times 10^{-7}$ for 40 nm particle rings and $\phi < 5 \times 10^{-8}$ for 15 nm particle rings) no ring is left on the substrate.

The superficial reason for the weak ϕ-dependence is the increasing porosity of the ring with decreasing concentration. Figure 10 shows SEM micrographs of rings

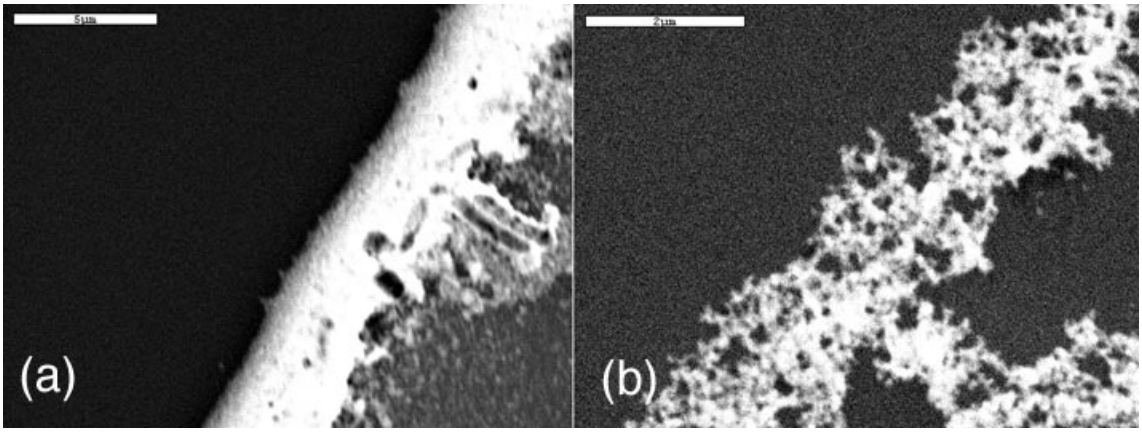

Figure 10 Morphology of gold rings. Scanning electron microscope images of rings formed from a drop with an initial volume fraction of (a) 5×10^{-4} and of (b) 5×10^{-7}. While the higher concentration forms a solid ring, the lower concentration drop forms a wispy ring. The scale bar is 5 μm in (a) and 2 μm in (b).

formed from a $\phi = 5 \times 10^{-6}$ solution (on the left) and a $\phi = 5 \times 10^{-7}$ solution (on the right). The ring formed from the high concentration colloid is densely packed whereas the ring formed from the low concentration colloids is mostly filled with voids. I believe that the process of diluting the original colloidal suspension with deionized water increases the Debye screening length to such an extent that incoming particles cannot penetrate the sparsely filled ring because of electrostatic repulsion. If so, diluting the colloid with a saline solution should eliminate this problem.

I was not able to determine if the absence of a ring at low concentrations is due to the ring not forming, or to a disturbance occurring during or after the drop dries. During the final step of the fabrication process the remaining liquid must be removed from the drop. During the first trials this was accomplished by sucking up the liquid with a pipette. I found, however, that this destroyed the ring. Letting the

drop dry on its own is undoubtedly gentler on the ring (rings are left where previously the pipetting destroyed them). The earlier experience suggests that it is plausible that the stresses on the ring during drying are too great for a thin ring to withstand.

CHAPTER 4

PATTERN FORMATION

The focus of the previous section was the pinning force on the contact line exerted by deposited solute. During this early stage of the drop's life the pinning force is so large that it is solely responsible for the contact line behavior. Uncomplicated constraints produce simple structures: a ring.This section shifts the focus to the events that occur after the contact line separates from the ring. Dewetting and pinning forces are of comparable strength during this stage. Here I will show that the competition between these two forces leads to complicated yet organized behavior.

As in the self-pinning experiments, the observations that follow are of drops of colloidal microspheres drying on a freshly cleaved mica surface. (Experiments conducted using a cleaned, optically-flat, silicon substrate gave similar results). The additional step of briefly centrifuging the 0.1 μm sample before use was performed to remove large particles ($\sim 1\mu$m) because otherwise the experiments were irreproducible. The experimental control parameters were particle size, solute concentration, surfactant concentration, ionic strength, and polydispersity of particle size. All observations were done with the aid of a fluorescent microscope. Therefore, the gray level in the images that follow is proportional to the number of particles at a given point with white corresponding to the largest value.

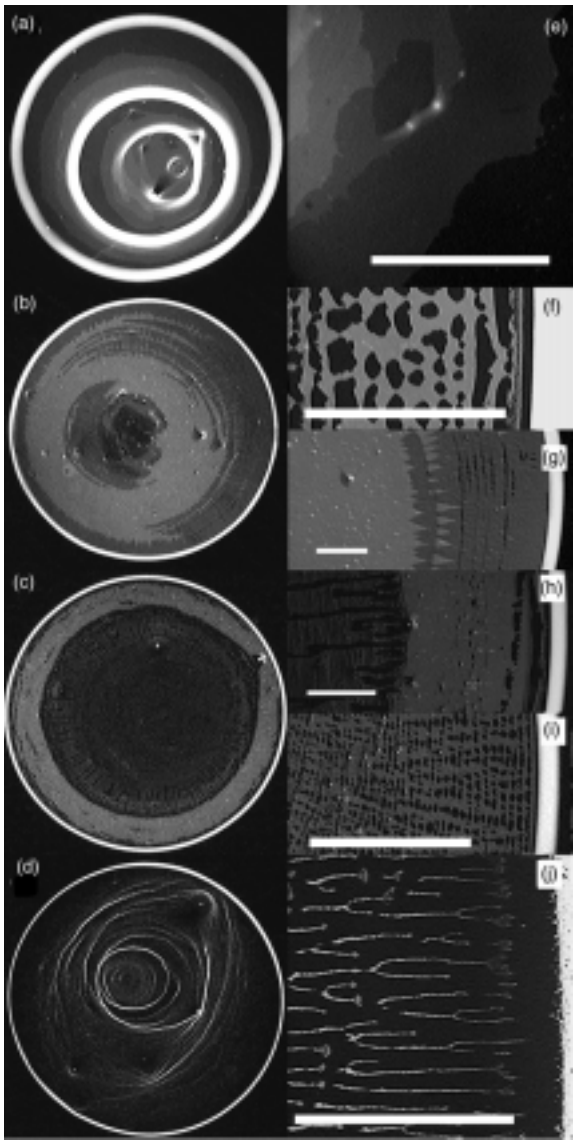

Figure 11 Deposition patterns left by drop containing 0.1 μ. Photographs of the deposit left by drops containing 0.1μ microspheres at various concentrations dried on mica. The gray-scale indicates the density of particles in a given area with white corresponding to the highest value. The left column shows the entire deposit for initial volume fraction (a) 1%, (b) 0.25%, (c), 0.13%, and (d) 0.063%. The diameter of these drops is approximately 6 mm. The right column shows a closeup of a deposit made from the same concentration as the deposit depicted to its immediate left; in some cases, multiple closeups for a single concentration are shown. The scale bar is 500 μm in frames (f) through (i) and 250 μm in frame (j).

4.1 Patterns with 0.1μm particles

Arranged top to bottom in order of decreasing concentration Fig. 11 shows the deposit resulting from dried drops of different initial concentration of 0.1μm microspheres. The left-hand column shows a complete picture of the deposit whereas the right-hand column shows only magnified fragments.At the scale of the whole drop a bull's-eye-like pattern is visible. In (a) there are four well defined concentric rings. In (b) and (c) the interior shows concentric marks but they are qualitatively different from those of (a). In (d) again the inner rings are strong though they are finer, less complete, and less organized than those in (a). The rings shown in (a) and (d) form when the contact line is pinned long enough that a large contact line deposit can form. Thus these rings chronicle the moments of arrested contact line motion.In contrast, direct observation of the deposition process leading to (b) and (c) shows that the rings in these cases are formed while the contact line is moving.

Magnifying the deposits reveals yet more structure. At the highest concentration (frame (e)), the space between the inner rings is coated by multiple layers of microspheres that are deeper in the vicinity of a ring; the deepening deposit heralds, and perhaps causes, the pinning episode during which a ring is formed. For ϕ =0.25% (frames b, f, and g) the interior of the deposit is coated with a layer of microspheres with a thickness that varies between one and two particles. The transition from a one and a two particle layer, indicated by the a step-like increase in brightness, has

a saw-toothed shaped pattern pointed radially outward (Fig. 11(f)). However, the transition from a two to a one layer deposit is abrupt as can be seen from the termination of the outermost saw-toothed front. The saw-toothed front is caused by a piece-wise transition to a double layer film. First, a few points along the contact line begin to produce two layers. As the contact line retreats, the segments producing double layers extend along the contact line, leaving a triangular-shaped deposit in their wake. Finally, the segments grow into one another so that the entire contact line deposits double layers. The piece-wise growth of the double layer and the abrupt return to a monolayer suggests that there is an energy cost to switching from a single to a double layer. If so, the saw-toothed front is an energetically inexpensive means of achieving two layer production because the distortion energy is localized to a few particle diameters along the contact line.

At ϕ =0.25% (Fig. 11(g)) and 0.13% (Fig. 11(h)) a grid-like pattern appears. It can exist concurrently with or separately from other patterns at these concentrations. The production of a grid appears to be an unstable version of single layer production. Direct observation of the contact line shows that parts of it move steadily and that the parts between these move in a stick-slip fashion. The steady moving segments lay down the radial lines of the grid and stick-slip segments produce nothing when moving and a ring when at rest; the combination of the radial lines and the rings forms a grid.Fig. 11(i) shows another type of pattern in which single layer deposition gives way to an even slower rate of deposition that does not achieve total

coverage and includes long, empty, radial grooves. Finally, at the lowest concentration ($\phi = 0.063\%$) another new mode appears in which radial spokes are produced (Fig. 11(j)).

4.2 Patterns with 1μm particles

Due to the difficulty of deducing the microscopic behavior of the particles when they are submicron in size and thus invisible with light microscopy, I focused on the behavior of drops with 1 μm particles.The patterns of deposit left when a drop dries are shown in Fig. 12 for different initial concentrations of 1μm-sized particles. In Fig. 12, frame (a) is the highest concentration and (f) is the lowest. There are distinct features and trends in the deposition patterns. The features may be grouped by distance from the center of the drop. Moving inward, the first zone is a featureless solid packing of particles. This is the initial ring formed before any depinning has taken place. The second zone consists of arch-shaped formations, the third zone is a mixture of half-formed arches and radial lines, and the central region is composed of apparently disorganized dots. The range of these phases as a function of concentration is plotted in Fig. 13. At high concentration all phases are present but as the concentration decreases, the mixed zone gains at the expense of the others and its composition.

A change in the velocity of the contact line might account for the different phases seen in the deposits. However, direct observation of the contact line shows that there is very little change in its speed. Another possibility is that the deposition

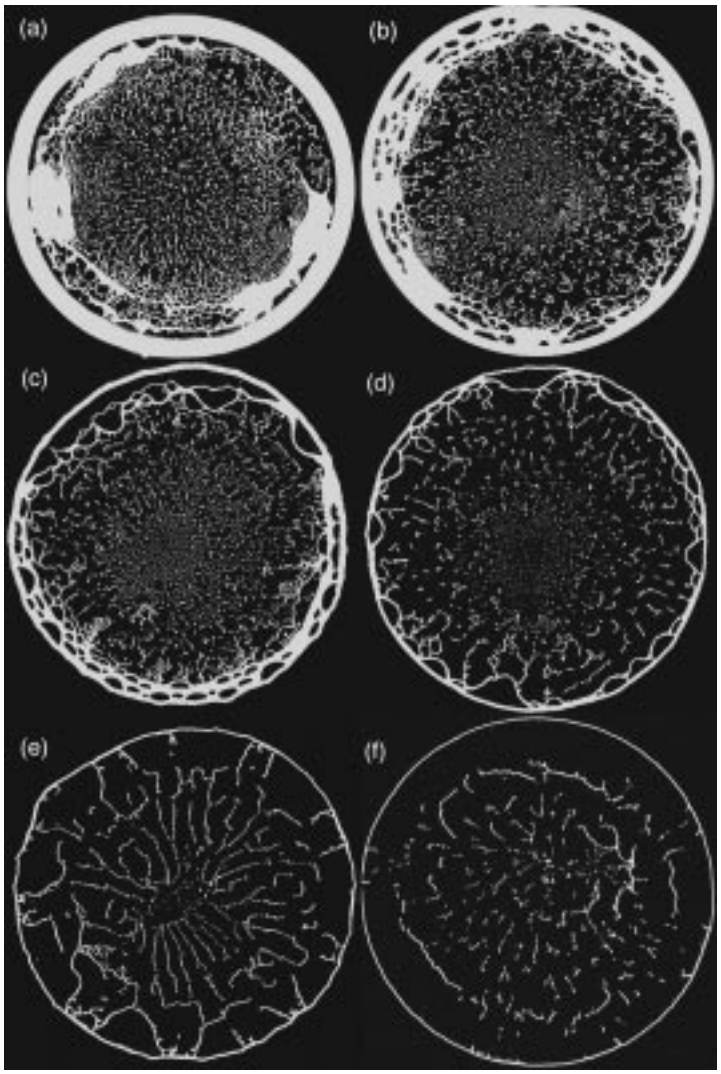

Figure 12 Deposit left by drops of 1μ microspheres dried on mica. The initial volume fraction reading from left to right and from top to bottom are 2.0%, 1.0%, 0.5%, 0.25%, 0.13%, & 0.063%.

rate at the contact line changes as the drop shrinks. This is consistent with a constant contact line velocity. Moreover, in 6 we showed that a gradient in the concentration develops and grows while the contact line is pinned. Therefore, the deposition rate would be altered as the contact line moved closer to the origin.

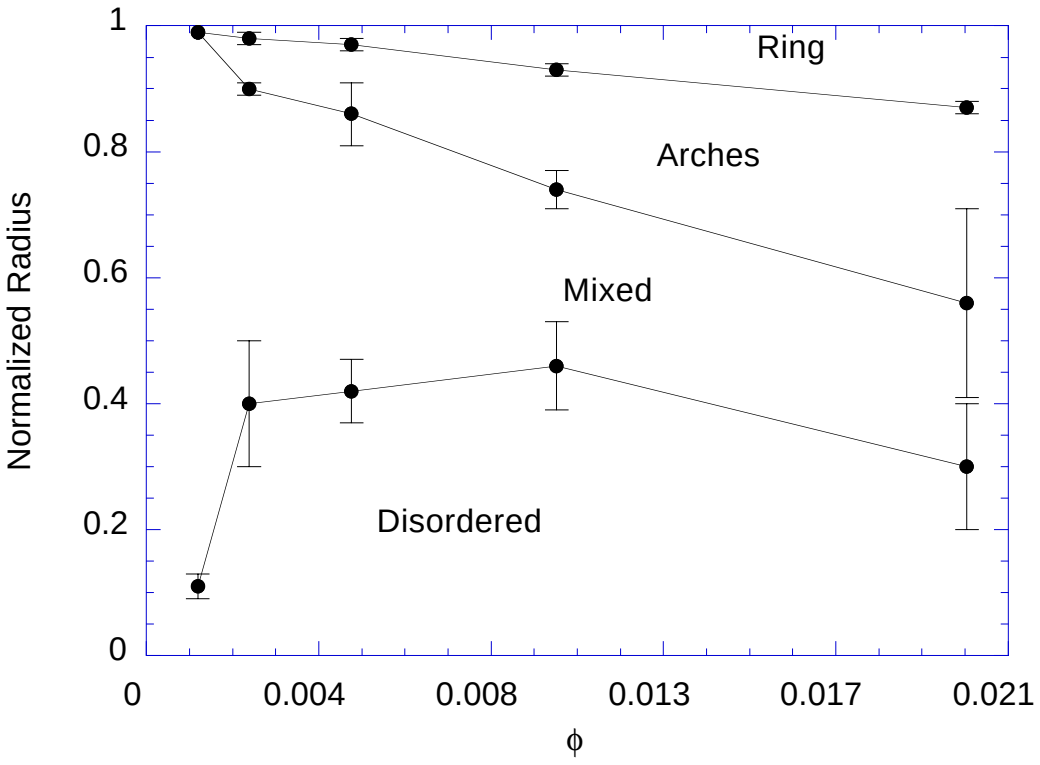

Figure 13 Size of phases in drops of 1 μm microspheres. The diagram indicates the range of each phase: ring, arch, mixed, and disordered phases. The radial position is normalized to 1 at the contact line.

The ring width as a function of concentration was quantified in the previous section. Here the focus will be on the other zones beginning first with the arches zone. I measured the size of individual arches from the resulting deposit of many drops; for each concentration a total of approximately 1000 measurements were taken. I took

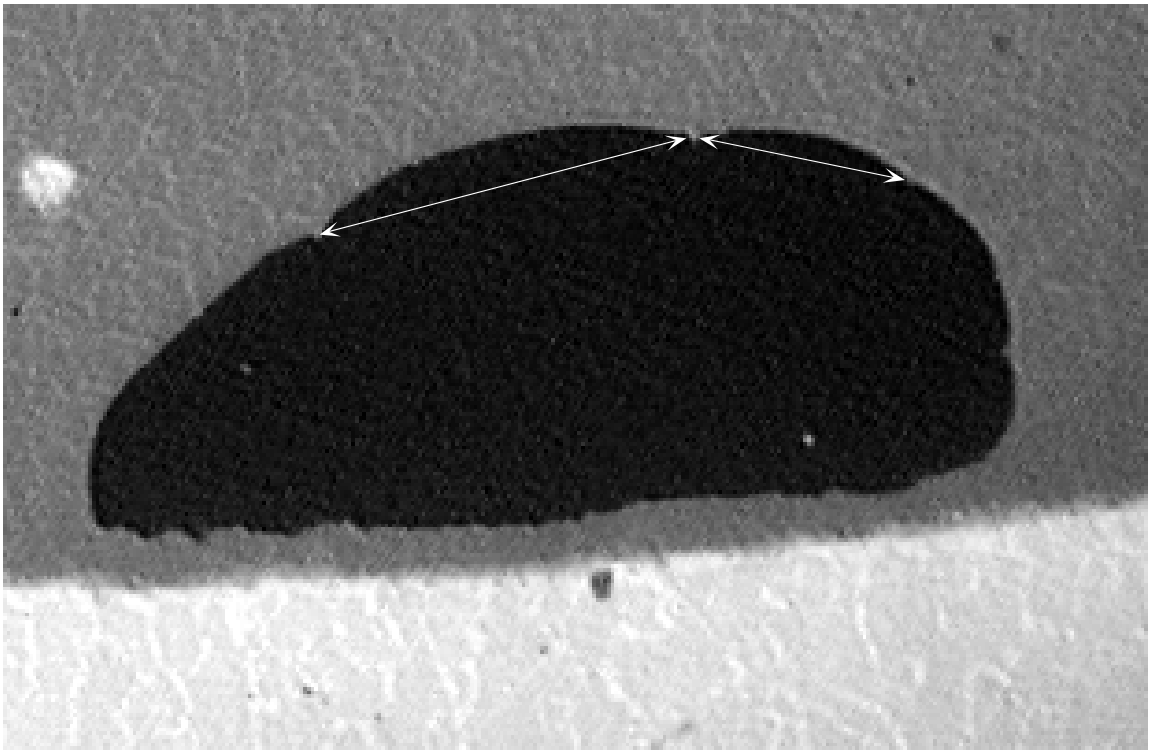

Figure 14 Measurement of sub-arches. A close-up view of a large arch shows that it is in fact composed of multiple sub-arches. Size of these smaller arches was measured as shown.

the greatest width of the arch as a measure of its size. Closer inspection of the larger arches showed that they were composed of multiple sub-arches; for these I measured the width of the sub-arch rather than width of the entire group. This procedure is shown in Fig.14. For the first four concentrations represented in Fig. 12, the arch measurements were binned by size and plotted in Fig. 15(a)-(d). Since there are no arches in drops with $\phi = 0.13\%$, instead I measured the perpendicular distance between spokes where they ran parallel to each other. The distribution function for these measurements is plotted in Fig. 15(e). For the concentration represented by Fig. 12(f) no length scale is apparent and so no measurements were made. There are two clear

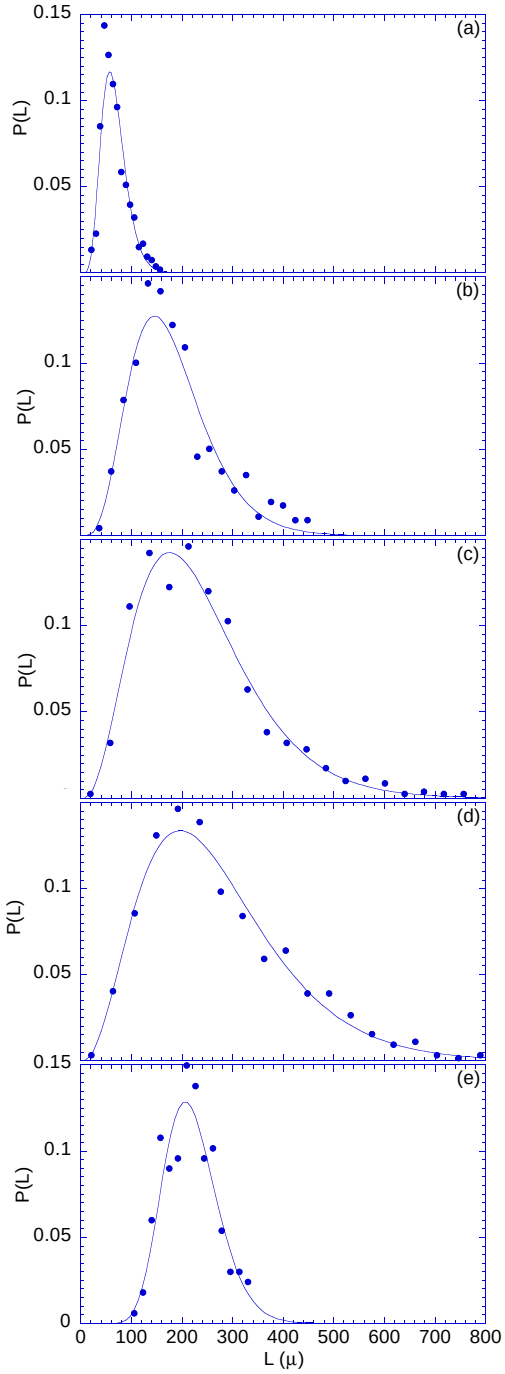

Figure 15 Distribution of arch size. Plot of the unnormalized distribution function of arch sizes. Plot (a) through (e) correspond to initial concentrations of 2.0%, 1.0%, 0.5%, 0.25%, & 0.13%, respectively.

trends apparent from the distribution function: for decreasing concentration the peak of the distribution shifts to a larger value and the width of the distribution, except for the lowest concentration, grows. The lowest concentration shows an abrupt narrowing of the distribution; this sudden jump corresponds to switching from measuring arch sizes to measuring the distance between radial lines. To extract the trends, the data in Fig. 15 was fit to the functional form $L^{\lambda}\exp(-L/a)$ from which I extracted the peak position and the full width at half height of the distribution. A plot of these parameters is shown in Fig. 16. The change in peak size is well fit by a linear function of concentration.

From observing the processes transpiring at the contact line a partial picture of the pattern formation process emerges. The outermost structure, the ring, was explained briefly in the introduction and in more detail elsewhere5, 6, 9, 10, 11, 12. The arches are formed by the process shown in Fig. 3: a hole is nucleated, the contact line begins to recede, but its growth is arrested by the accumulation of particles. Hole nucleation in nanometer-thick films has been previously observed 13, 14 and mechanisms for their formation have been proposed in 13 and 15. However, these mechanism are inapplicable to the micron-thick films present in my experiments. The growth of arch size with decreasing concentration may be plausibly explained by the fact that there are fewer particles with which to pin the contact line and this allows the arches to grow larger. By frame (e) there is an insufficient number of particles to stop the contact line from moving and the arches grow without bound;

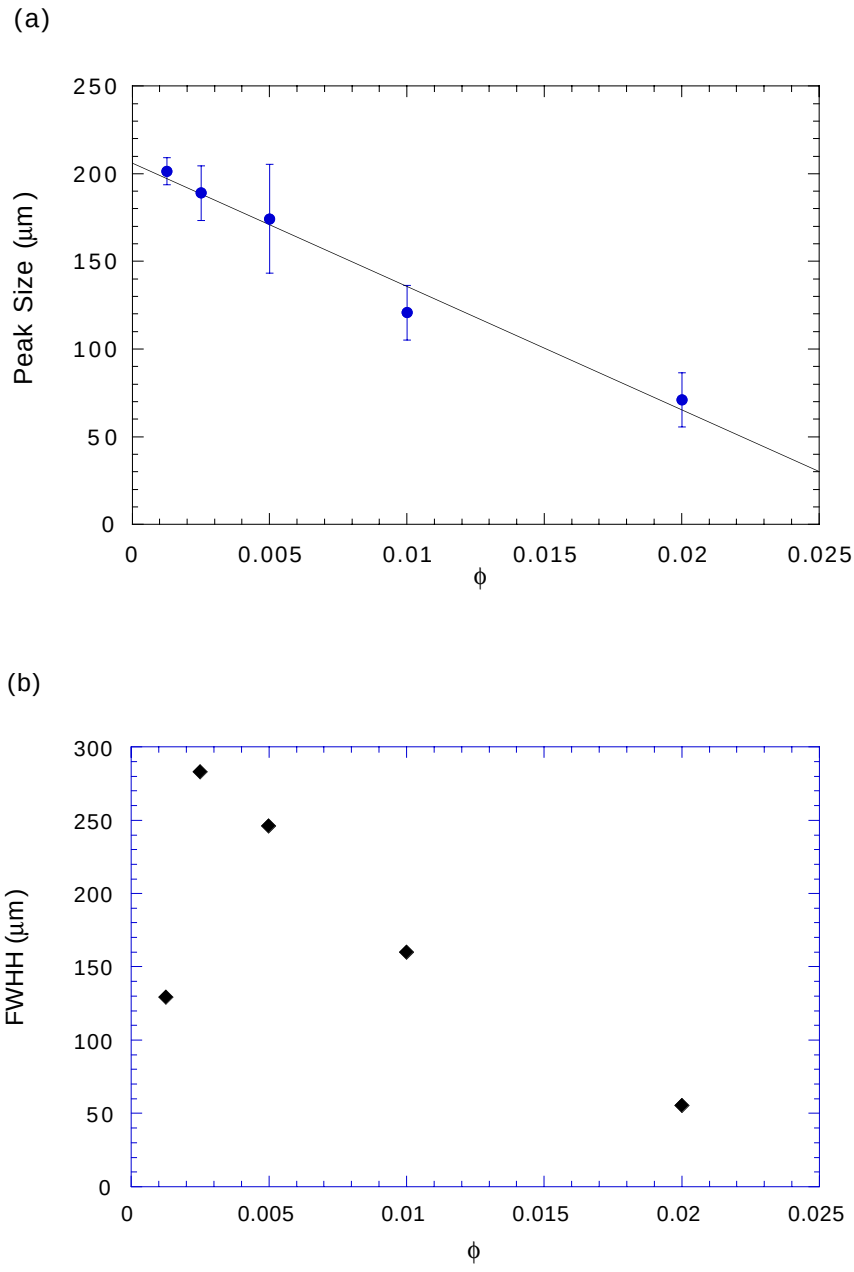

Figure 16 Parameters of distribution. (a) The most likely size of an arch versus concentration taken from the peak position in the curve of Fig. 15. (b) The full width at half height versus concentration of those curves.

this accounts for the absence of arches in frames (e) and (f). Ohara and Gelbart have previously proposed the same mechanism for pinning of the contact line by nanoparticles. They predict that $L \propto 1/\phi$ for a hole spreading in a film of uniform thickness and concentration. The result is not consistent with my data but it is not expected to hold given that a drop is not uniformly thick, that there are additional flows in a ring-forming drops, and that the concentration is not uniform.

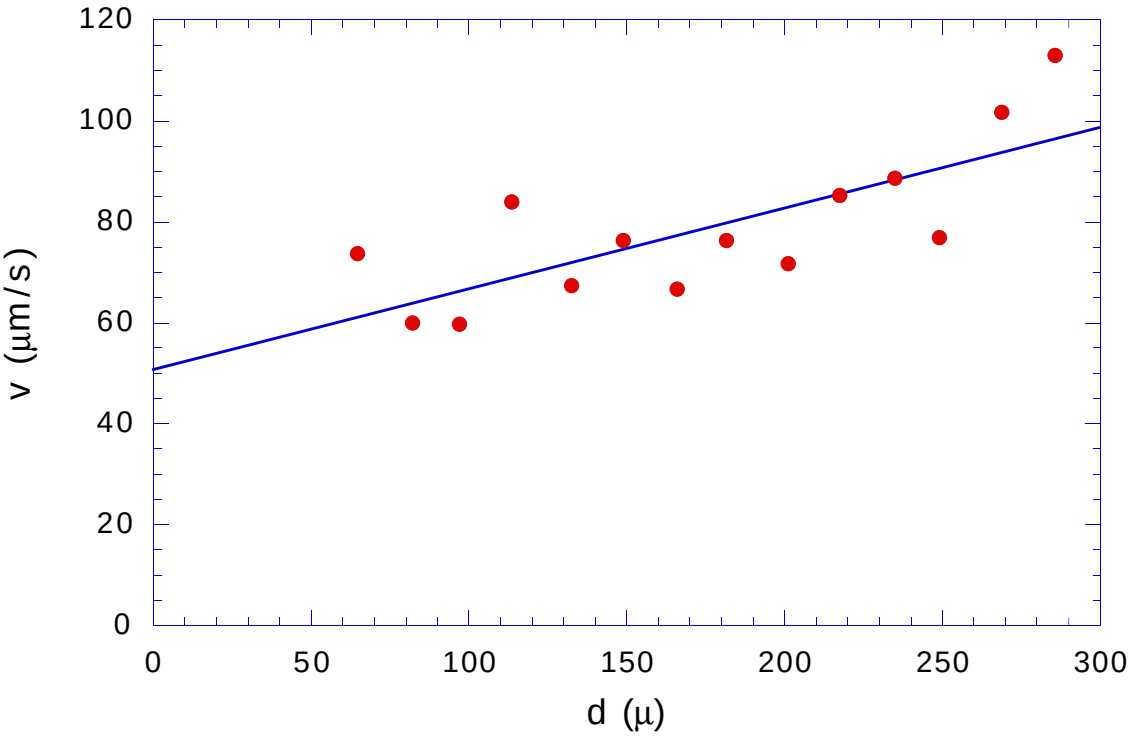

Figure 17 Dispersion relationship for contact line. The velocity of the contact line between two cusps versus the distance between the two cusps. The initial concentration of the drops was $\phi = 6.25 \times 10^{-4}$. The fit is to a linear equation which gives $v = 50.7 + 0.16d$ in units of μm/s.

The mixed zone begins when the number of holes times their average size becomes comparable to the circumference of the drop. Unlike the arch creation period

in which the majority of the contact line is pinned, large portions of the contact line become free to move. At high concentrations this motion is heavily constrained by the accumulation of particles and hence erratic. The half-formed arches develop when a small portion of the contact line is temporarily pinned. However, for lower concentrations the contact line organizes itself into a series of cusps that emit particles. This deposition appears to be a release of particles controlled so that there is no net accumulation at the contact line. During this type of motion, radial lines are formed. The ability of the contact line to do this is thwarted at higher concentrations because the influx of particles is overwhelming. As the concentration is lowered and fewer particles reach the contact line per unit time the ejection process can handle all the particles that arrive; this is the situation in Fig. 12(e). At even lower concentrations (Fig. 12(f)) the output from the cusps can exceed the influx of particles and the emission process becomes discontinuous leaving disjointed trails of particles which are nonetheless radially oriented.

In other pattern forming systems, such as solidifying alloys, the wavelength selection criterion depends on the velocity of interface. In order to determine if an analogous relation exists in drying drops, I measured the velocity of the minima between two cusps and the cusp-to-cusp distance during the stage when the radial spokes in Fig. 12(e) were generated. The data are plotted in Fig. 17 and they show only a very weak relation between the velocity and the cusp-to-cusp distance.

I also measured the shape of the interface to compare it with the shape expected from contact line elasticity 16 in the low velocity limit. For measurement purposes, I defined the contact line as the outline of the particles caught in the wedge of fluid next to the contact line. Using a fluorescent microscope and fluorescent dyed particles, I captured images of the contact line and extracted the outline of the macroscopic contact line. Since there was no predefined zero, I defined it as the line connecting the lowest point on each side of the cusp. An elaboration of this is shown in Fig. 18. The height of the cusp above the zero line is plotted against distance in Fig. 19 where the zero of the abscissa was chosen to achieve the maximum symmetry between the two sides. The data is well fit by an exponential function. This fit is better than the logarithmic fit expected from contact line elasticity. This discrepancy may be accounted for by viscous dissipation in the fluid, the interaction of the particles through capillary force 17, or deviations from the logarithm due to defect size.

4.3 Patterns from mixtures

The parameter space of the deposition patterns was further probed by combining colloidal microspheres with surfactant, salt, and microspheres of a different size. A sampling of the results is given below. It is clear that there are many control parameters and that there are many different deposition patterns.

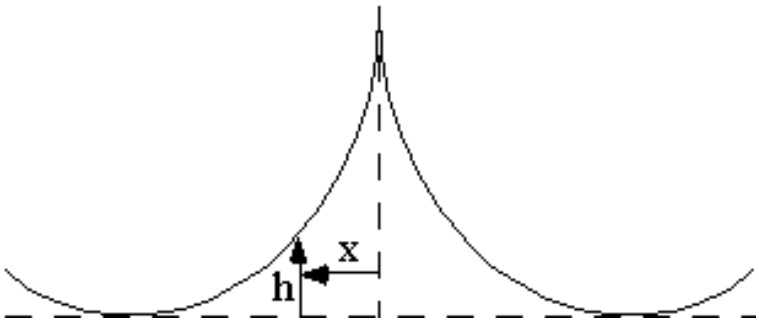

Figure 18 Shape of cusp measurement. Schematics of demonstrating contact line position measurement. The position of the contact line (the dashed line in the closeup) was inferred from the position of the microspheres. The zero height position was chosen as the segment connecting the two minima between a pair of cusps and the zero x position was chosen by finding the horizontal value at which the left and right hand parts of the curve are most symmetric.

The anionic surfactant sodium dodecyl sulphate (SDS) was added to the 0.1μm colloid. This was motivated by differences observed in the patterns left by drops of the same concentration but containing colloidal particles synthesized by different manufacturers. By the addition of surfactant to a surfactant-free sample I was able to produce similar patterns to those formed by other colloid brands. (The inexact match may be due to differences in the ionic strength.) In addition, I found a number of new patterns which are shown in Fig. 20. These patterns where made from a colloid with a fixed volume fraction of microspheres ($\phi = 0.0013$) but variable concentrations of SDS. During the production of these patterns the contact line sweeps from top to bottom in the images of Fig. 20.

Since the strength and range of the interaction between microspheres and between a microsphere and the substrate is determined by screening ions, I tried

altering the ionic strength of the solvent and observed the resulting deposition pattern. Starting with a 2% solid volume-fraction of 1 μm microspheres I diluted the sample down to ϕ =0.25% with a NaCl and water solution. The images shown in Fig. 21 are the patterns left when a drop of this mixture is dried on mica. The molarity of the solution used to make (a) was 0 M, (b) was 0.01 mM, (c) was 0.1 mM, and (d) was 1 mM. From these images it is clear that the addition of salt radically alters the resulting deposit. It would be interesting to know if this is due to a change in the

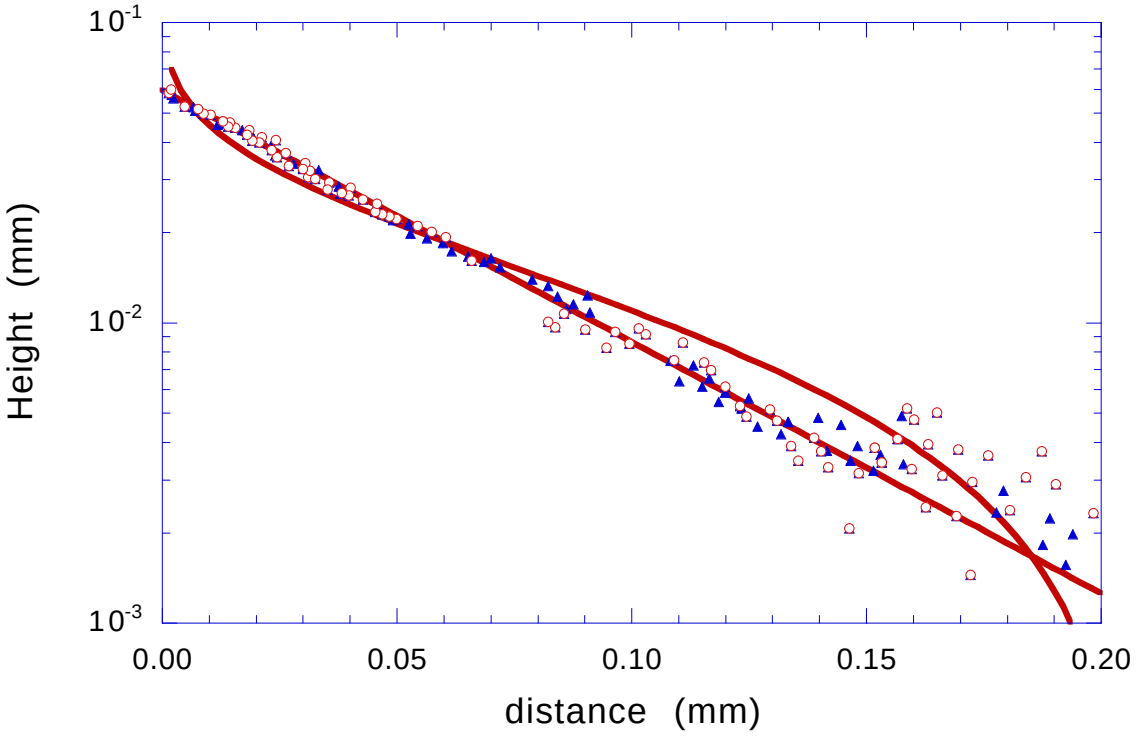

Figure 19 Shape of contact line cusp. The position of the contact line relative to the zero point versus distance plotted on a log-linear scale. The straight solid line running through the data is a fit to an exponential and the curved solid line is a fit to a logarithm.

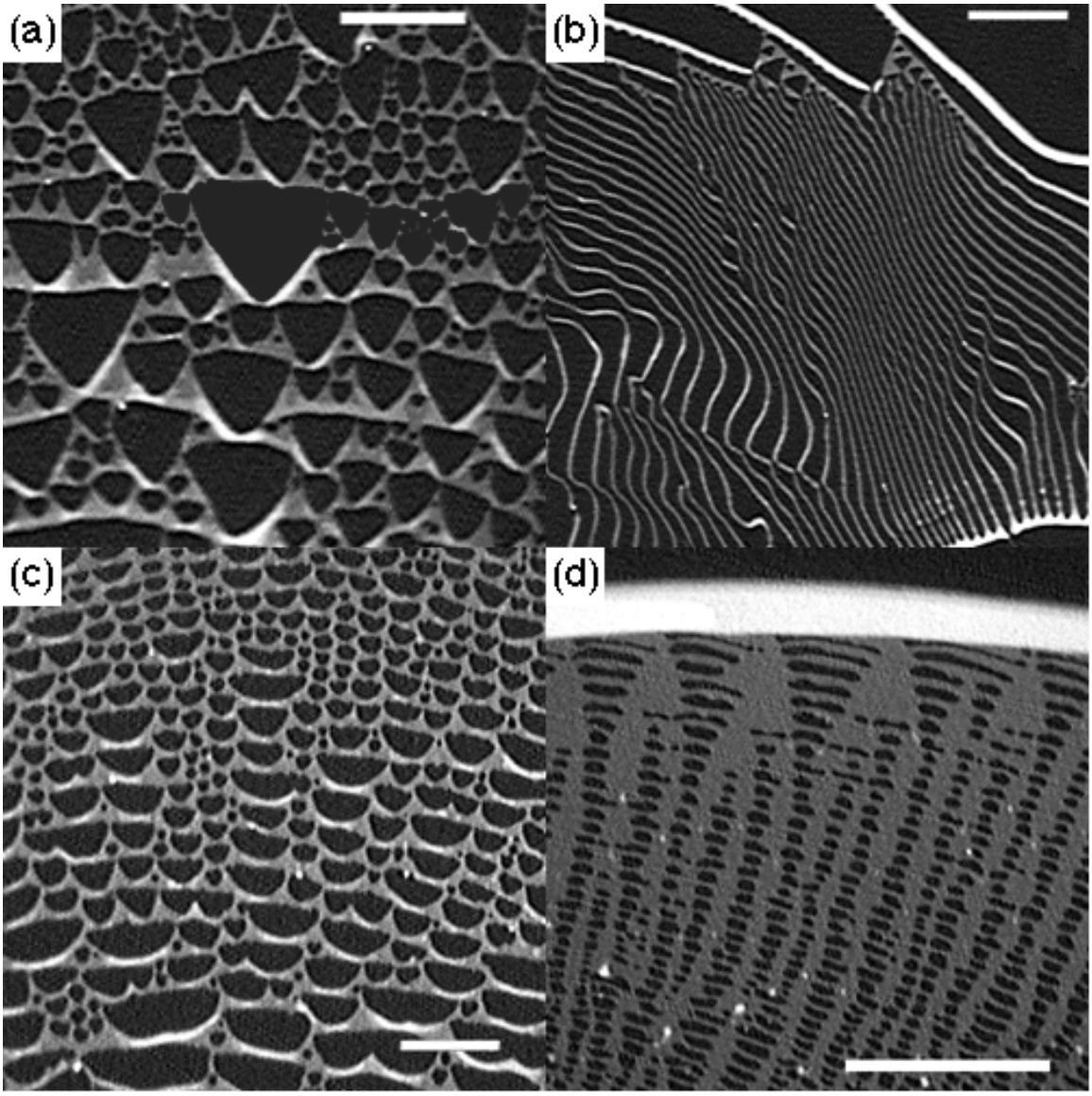

Figure 20 Deposit left by 0.1μ microspheres of 0.5% initial volume fraction when SDS surfactant is added. The center of the drop lies below the image so that the contact line moved from top to bottom. In each image the scale bar corresponds to 50 μ. In frames (a) through (d) the concentration of surfactant is 8.1×10^{-4} M, 4.3×10^{-4} M, 1.4×10^{-4} M, and 4.8×10^{-5} M, respectively.

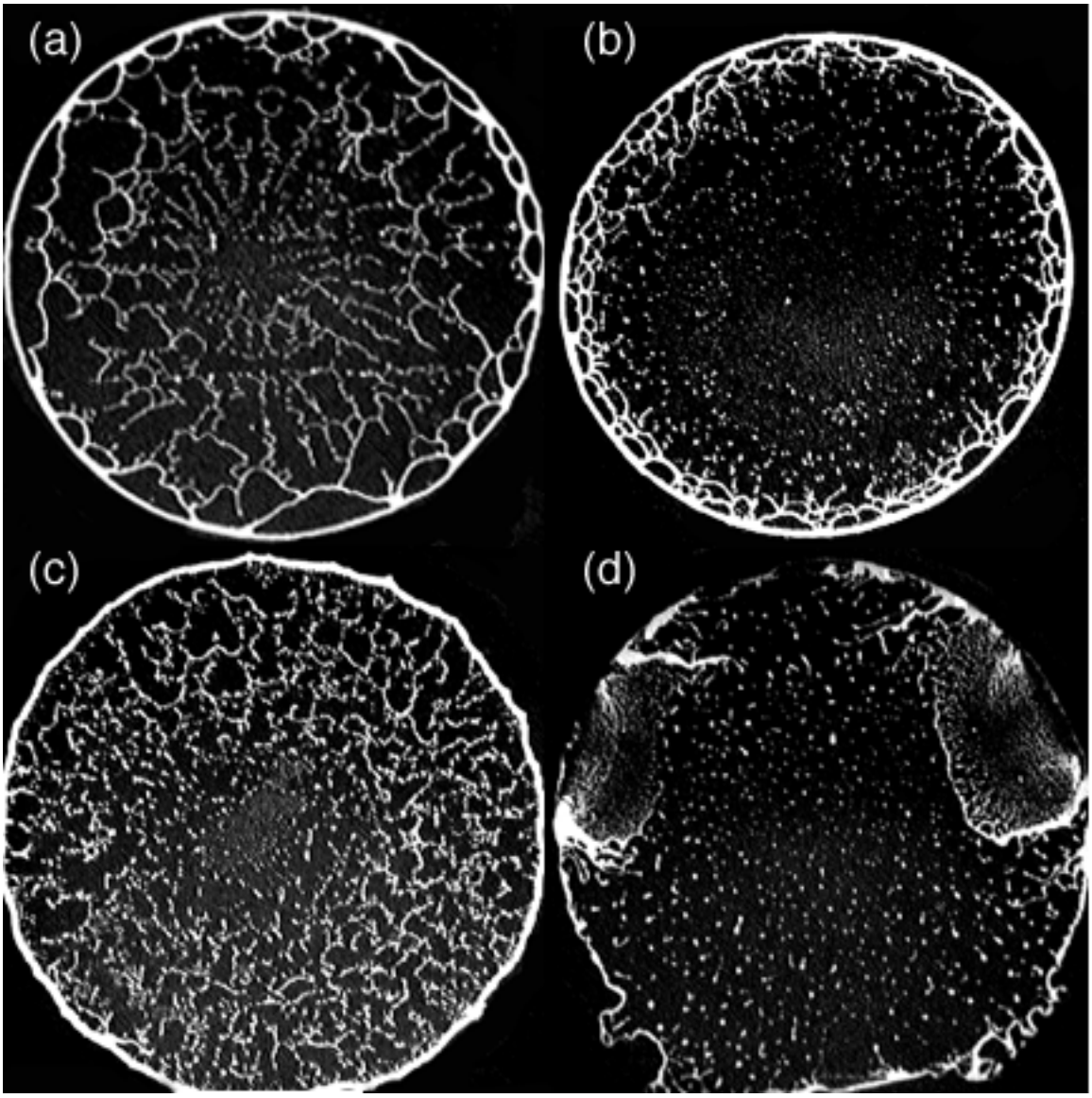

Figure 21 Deposit left by a 0.25% solid volume-fraction of 1μ microspheres in solvent with different ionic strength (see text).

particle-particle or particle-substrate interaction, or to the pinning effects of deposited salt.

Last, I investigated the effect of combining 0.1 μm and 1 μm microspheres. Two of the most interesting deposits generated by this binary combination are shown

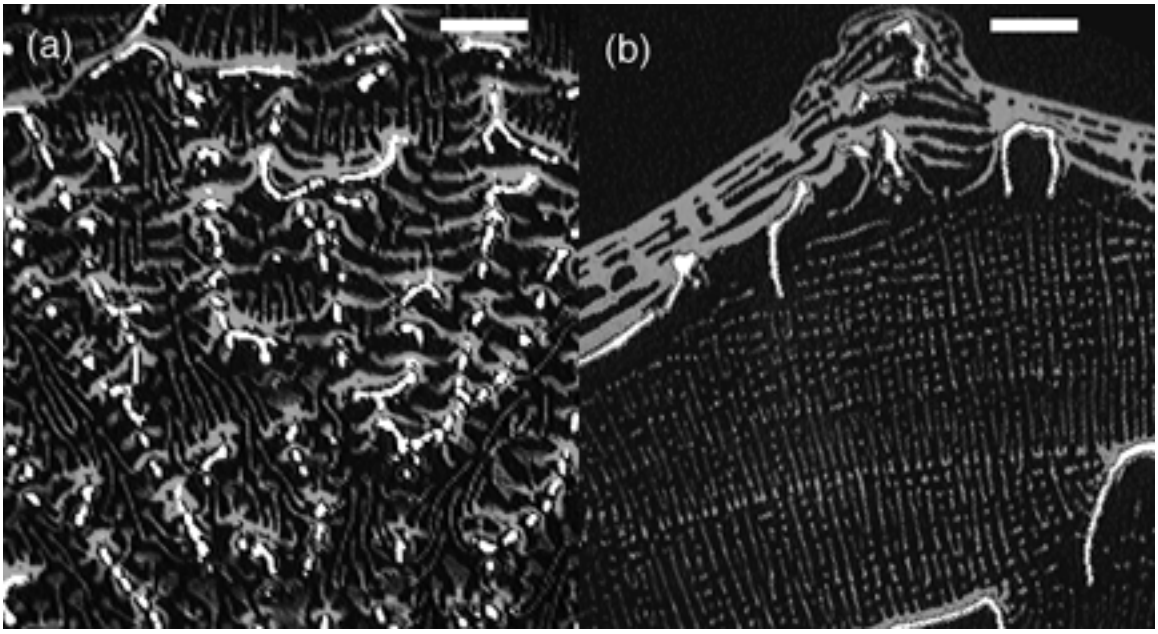

Figure 22 Deposit left by mixture of 0.1 μm and 1 μm microspheres. The mixture for these images is 50/50 mixture of 0.1μm and 1 μm microspheres diluted down to a volume fraction of 0.125% for (a) and 0.0625% for (b). The bright parts of the deposit correspond to deposits of 1 μm microspheres and the gray parts correspond to deposits of 0.1 μm microspheres. The scale bar corresponds to 200 μm.

in Fig. 22. These deposits were formed from a 1 to 1 mixture of 0.1 μm and 1 μm colloid with an initial volume fraction of 0.125% and 0.0625%.

CHAPTER 5

CONCLUSION

The major results presented here are that the contact line can self-pin, that the competition between this pinning and dewetting give rise to pattern formation, and that these patterns exhibit evidence of wavelength selection. A drying drop is a new, rich, and unexplored example of a pattern forming system. It can be controlled in numerous ways–solute concentration, particle size, surfactant concentration, ionic strength, and particle mixtures were partly treated here. All the tools that have been developed to treat nonlinear systems far from equilibrium can be brough to bear on this problem. It will be interesting to know if this system fits the standard paradigm of pattern formation.

Investigating pattern formation in drying drops is appealing because a great deal is known about contact line behavior and so it ought to be theoretically tractable, and it is a relatively simple experimental system. However, some fundamental experimental and theoretical problems must first be tackled. On the experimental side, the circular geometry of a drop is too difficult to work with. The phases shown in Fig. 13 are most likely a manifestation of this problem. In addition, there is the problem of defining experimentally the unperturbed state. Furthermore, the free drying conditions do not provide sufficient control on the kinetic processes in the system. It

is clear that an analog of the drop with a linear geometry must be made. The result of such experiments ought to provide the stimulus that directional solidification experiments provided for the dendritic growth problem 18.

On the theoretical side, the most obvious unknowns are (1) the flow within a spreading drop of volatile fluid and (2) the wavelength selection mechanism. The spreading of volatile liquids is a research problem in its own right. However, it appears to be an essential prerequisite for understanding the patterns in drying drops because the flow in the drop determines the distribution of solvent. Though there has been some progress on this spreading problem 19, 20, 21 there is as of yet no widely-held consensus. The wavelength selection problem is completely open because the result presented here are the first of its kind.

Last, in chapter three I reported my attempts to create microscale structures. While I find that it is possible to make repeatable structures 500 nm wide, my attempts to make smaller rings was thwarted by the increasing porosity of the ring. I was not able to ascertain the cause of this and an explanation must be preceeded by further experimental work.

APPENDIX: RING WIDTH CALCULATION

To model the shape of the deposit at the contact line, and in particular to obtain its width versus time, the drop is separated into three regions (I, II, & the ring) as shown in Fig. 23. Regions I and II are composed of solution and the ring is a solid formed from the solute with packing fraction p. The total volume of liquid at any given moment is:

$$V_L = V_I + V_{II} + (1-p)V_r \simeq \pi R^2 h + \frac{\pi R^3 \Theta}{4} \tag{A.1}$$

where V_r is neglected because it is small compared to V_I and V_{II}, Θ is assumed to be small, and the shape of region I is assumed to be a thin spherical cap. Furthermore, the volume of the drop is assumed to decreases linearly so that

$$V_L(t) = \frac{\pi R^3 \theta_c}{4}(1 - t/t_f) \tag{A.2}$$

where θ_c is the *initial* contact angle. From Fig. 23 we get the geometrical relation:

$$\frac{dh}{dw} = \tan\Theta \simeq \Theta \tag{A.3}$$

The ring grows inward at the rate dw/dt. Therefore, the volume of the ring changes as solute is added and

$$\frac{dV_r}{dt} = 2\pi R h \frac{dw}{dt} \tag{A.4}$$

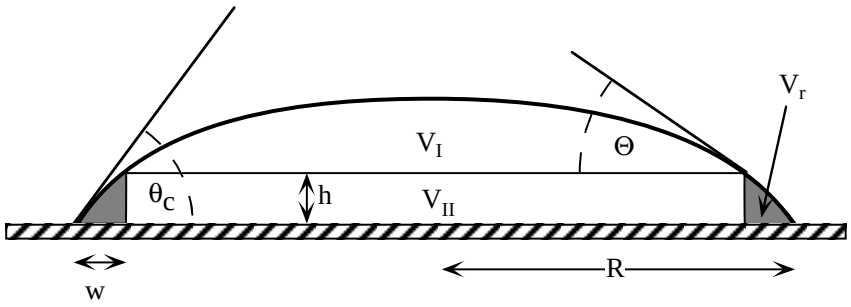

Figure 23 Regions of the drop. Diagram depicting the separation of a drop into three regions. Region I is shaped like a spherical cap and region II is a cylinder. The shape of ring deposit is determined by the equations in the text. At any given time the interface between the ring and the solution is located at w from the contact line and is h high. The aspect ratio is greatly exaggerated.

Using Eq. 2.2 gives

$$\frac{dV_r}{dt} = p^{-1}\frac{\pi R^3 \theta_o}{4}\phi\frac{(1-(1-t/t_f)^{3/4})^{1/3}}{(1-t/t_f)^{1/4}} \tag{A.5}$$

Putting together Eqs. A.1, A.2, A.3, & A.4 and introducing the non-dimensionalized variables $x \equiv 4w/R$, $y \equiv 4h/(\theta_o R)$, and $\tau \equiv t/t_f$ we arrive at the pair of coupled ordinary differential equations that govern the shape of the ring:

$$\frac{2\phi}{p}\frac{(1-(1-\tau)^{3/4})^{1/3}}{(1-\tau)^{1/4}} = y\frac{dx}{d\tau} \tag{A.6}$$

$$(1-\tau-y)\frac{dx}{d\tau} = \frac{dy}{d\tau} \tag{A.7}$$

It is clear from the absence of R from non-dimensional form of the equations that w will scale with R. For calculation purposes, I assume that $p = 0.656$, and that the initial conditions are that $w(t=0) = 0$ and $h(t=0) = 0$. The equations were integrated numerically to achieve the conversion of the time data in Fig. 4 into the width data displayed in Fig. 5.

REFERENCES

[1] T. Young, *Philos. Trans. R. Soc* **95**, 65 (1805).

[2] P. G. de Gennes, *Rev. Mod. Phys* **57**, 827 (1985).

[3] E. L. Decker and S. Garoff, *Langmuir* **13**, 6321 (1997).

[4] R. Johnson and R. Dettre, p. 112 in *Contact Angle, Wettability and Adhesion*, edited by F. M. Fowkes, Advances in Chemistry Series, N0. 43 (American Chemical Society, Washington, DC, 1964).

[5] R. D. Deegan, O. Bakajin, T. F. Dupont, G. Huber, S. R. Nagel, and T. A. Witten, *Nature* **389**, 827 (1997).

[6] R. D. Deegan, O. Bakajin, T. F. Dupont, G. Huber, S. R. Nagel, and T. A. Witten, submitted to PRE.

[7] G. D. Nadkarni and S. Garoff, *Europhys. Lett.* **20**, 523 (1992).

[8] C. Bourgès-Monnier and M. E. R. Shanahan, *Langmuir* **11**, 2820 (1995).

[9] F. Parisse and C. Allain, *J. Phys II* **6**, 1111 (1996).

[10] F. Parisse and C. Allain, *Langmuir* **13**, 3598 (1996)

[11] E. Adachi, A. S. Dimitro, and K. Nagayama, p.419 in *Film Formation in Waterborne Coatings* Edited by T.Provder, M. A. Winnik, and M. W. Urban (American Chemical Society, Washington, DC, 1996).

[12] E. Adachi, A. S. Dimitro, and K. Nagayama, *Langmuir* **11**, 1057 (1995).

[13] P. C. Ohara and W. M. Gelbart, *Langmuir* **14**, 3418 (1997)

[14] M. Elbaum and S. G. Lipson, *Phys. Rev. Lett.* **72**, 3562 (1994).

[15] N. Samid-Merzel, S. G. Lipson, and D. S. Tannhauser, *Phys. Rev. E* **57**, 2906 (1998).

[16] J. F. Joanny and P. G. de Gennes, *J. Chem. Phys.* , 552 (1984)

[17] P. A. Kralchevsky, V. N. Paunov, I. B. Ivanov, and K. Nagayama, *J. Colloid Interface Sci.* **151**, 79 (1992).

[18] J. S. Langer, *Rev. Mod. Phys.* **52**, 1 (1980).

[19] L. M. Hocking, *Physics of Fluids* **7**, 2950 (1995).

[20] M. Elbaum, S. G. Lipson, and J. S. Wettlaufer *Europhys. Lett.* **29**, 457 (1995).

[21] C.-M. Lin, R. M. Ybarra, and P. Neogi, *Adv. Colloid Interface Sci.* **67**, 185 (1996)